JOURNAL OF AIRCRAFT
Vol. 31, No. 3, May–June 1994

# Physics of Coanda Jet Detachment at High-Pressure Ratio

Kenneth C. Cornelius* and Gerald A. Lucius†
*Wright State University, Dayton, Ohio 45458*

**Experimental measurements of surface pressure for an underexpanded two-dimensional supersonic Coanda flow with static conditions exterior to the jet flow was obtained for a fixed slot height to a radius ratio of 0.04. The data demonstrate that an oblique shock forms near the jet exit plane which vectors the jet flow from the curved surface at a pressure ratio of 7.6. The jet detachment occurs at a pressure ratio which is a function of the ratio of slot height to cylinder radius. An increase in the pressure ratio to 11.5 before jet detachment has been demonstrated by the translation of the upper wall providing for a converging-diverging geometry. The physics of the Coanda expansion and the jet detachment are qualitatively described using an optical schlieren system. A compressible inviscid model was derived analytically to demonstrate the variation in Mach number and surface pressure as a function of the geometric parameters with increasing pressure ratio.**

## Nomenclature

$A^*$ = linear dimension of throat for nozzle, 0.1 cm
$C_d$ = discharge coefficient
$C_p$ = pressure coefficient
$C_{pt}$ = surface pressure coefficient
$C_\mu$ = $(\dot{m}V_j/QA_{\text{ref}})$, nozzle blowing coefficient
$c$ = chord of wing
$F_t$ = isentropic force
$F_x$ = axial force
$F_y$ = side force
$I$, $II$ = right and left running waves
$k$ = ratio of specific heats
$M$ = Mach number, $V/(kRT)^{0.5}$
$M^*$ = Mach number based on $T^*$
$\dot{m}$ = nozzle mass flow rate
$P^*$ = nozzle throat pressure
$P_a$ = atmospheric pressure
$P_r$ = pressure ratio, $P_0/P_a$
$P_{re}$ = effective jet pressure ratio
$P_0$ = total plenum pressure
$R$ = radius of cylinder, $R_0$ = 2.0 cm
$R_d$ = Reynolds number based on $A^*$ ($3.2 \times 10^4$)
$R_\infty$ = outer radius of fully expanded jet
$(r, \theta)$ = cylindrical coordinate system
$T_0$ = plenum total temperature
$V_\theta$ = tangential velocity
$X$ = length extension of wall
$(x, y)$ = coordinate axis
$\theta$ = angle around cylinder, deg
$\theta_s$ = momentum vector angle
$\nu_{pe}$ = Prandtl Meyer expansion angle

## Introduction

THE presence of a jet attachment limit for Coanda-type devices has been quantified during research on the generation of high-lift devices, including circulation control wings (CCW) and the tangentially blown flap with noncircular trailing edges. Researchers[1–12] have reported that jet flow detachment is brought about by large slot heights, high-pressure ratios across the nozzle, and small radii for the Coanda surface. From this data, it was postulated that the detachment phenomenon was related to a sufficiently large pressure rise due to recompression of the supersonic jet. The preceding research indicates that the compressible flow performance of CCW sections is probably dependent not only on local trailing-edge geometry and characteristics of the underexpanded jet, but also is quite strongly influenced by the external freestream which can decrease the local static pressure at the jet exit plane. This can be significant for the two-dimensional jet imbedded at the trailing edge of the airfoil for CCW applications, or at the side of the fuselage[13] for vortex flow control, where a significant $-C_p$ exists at the exit plane of the jet from the external aerodynamic flow, thus increasing the effective $P_r$.

The current problem for a two-dimensional, underexpanded Coanda jet with high-pressure air passing through the throat region of a two-dimensional slot, and then expanding supersonically around a curved surface, is the bifurcation or change in state of the flow which occurs at a high $P_r$ for a given slot height to radius ratio $A^*/R$. Once the threshold in critical $P_r$ is surpassed, the jet flow is vectored from the surface. Hence, the Coanda jet loses the effectiveness for boundary-layer control. For CCW applications, the Mach number for a streamline above the jet flow must remain subsonic[5–8] to maintain an increase in the lift coefficient with additional jet momentum. Both of these effects limit the maximum lift coefficient with an increase in the freestream Mach number.

## Experimental Arrangement

The supersonic Coanda flow around a cylinder was examined experimentally to highlight the physics and ascertain the pertinent variables which influence this problem. An ex-

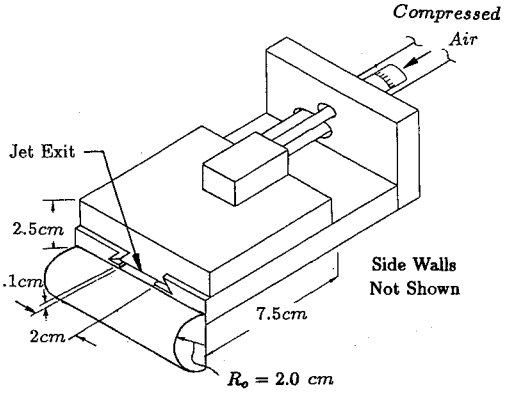


**Fig. 1 Schematic of experimental arrangement.**

Received Jan. 4, 1993; revision received April 28, 1993; accepted for publication April 28, 1993. 

*Assistant Professor, Department of Mechanical and Materials Engineering. Senior Member AIAA.
†Graduate Student. Member AIAA.

periment was undertaken to quantify the flow detachment at higher $P_r$ values. A circular cylinder with a radius of 2.0 cm was designed with static pressure taps at 5-deg increments. The cylinder was connected to a plenum which had a converging geometry to the jet exit plane with a two-dimensional slot height of $A^* = 0.1$ cm, which provided for an aspect ratio of 20 for the jet. This geometry provided a fixed slot height to radius ratio $A^*/R = 0.04$. Side walls were designed and connected around the circumference to achieve a higher effective aspect ratio. The experimental arrangement is shown in Fig. 1. The plenum was machined into a dovetail traverse to facilitate the movement of the upper wall. This allowed an examination of the influence of the converging-diverging nozzle geometry at different $P_r$ values. The cylindrical wall static pressures were measured for variable wall extensions on each nozzle configuration. Pressure transducers were used for the plenum total pressure and measurement of the wall static pressure, and were calibrated using a standard pressure source. A barometer was used for the measurement of the local atmospheric pressure. The parameter $x/A^*$, which represents the nondimensional extension of the top wall, was varied from a value of 0 to the limit at $x/A^* = 8$. This experimental procedure was followed for each $P_r$. Using a calibrated venturi, the $C_d$ was measured as 0.94 at $P_r = 2.0$, and increased to 0.95 at $P_r = 11$ for the two-dimensional nozzle. The extended wall did not influence the $C_d$ value for the $P_r$ values under consideration. A monochromatic light source with associated optics was utilized for a schlieren system. This technique was used for qualitative flow visualization using photographs of the density gradients produced in the supersonic regime of the Coanda jet expansion flowfield.

## Approximate Theory and Two-Dimensional Wave Physics

A theoretical model that treats the flow as an isentropic expansion to the local static pressure provides for a cursory examination of the relevant parameters which impact this problem. The theory neglects the surface shear stress and the circumferential pressure and velocity gradients. The framework of these assumptions allows an analytical expression to be formulated. The theoretical results are presented to highlight the interaction between the physical variables of importance for this problem. The radial momentum equation, neglecting gradients of the flow in the $\theta$ direction, becomes

$$\frac{\delta P}{\delta r} = \frac{\rho V_\theta^2}{r} \tag{1}$$

This equation specifies that the centrifugal force must be balanced by the local radial pressure gradient, where for an ideal gas

$$\rho V^2 = kPM^2 \tag{2}$$

For isentropic flow, the Mach number can be expressed in terms of the pressure as

$$M^2 = \frac{2}{k-1}\left[\left(\frac{P}{P_0}\right)^{(1-k/k)} - 1\right] \tag{3}$$

Integrating Eq. (1) from the surface to the radius $r$

$$\int_1^{\bar{r}} \frac{\delta_{\bar{r}}}{\bar{r}} = \int_{\bar{P}_{(1)}}^{\bar{P}_{(\bar{r})}} \frac{\delta \bar{P}}{\frac{2k}{k-1}\bar{P}\left[\bar{P}^{(1-k/k)} - 1\right]} \tag{4}$$

The pressure distribution as a function of the radial coordinate can be expressed as

$$\bar{P}(\bar{r}) = \left[\frac{C(\bar{r})^2(R_0/R_\infty)^2}{C(\bar{r})^2(R_0/R_\infty)^2 - 1}\right]^{(k/1-k)} \tag{5}$$

where

$$C = \frac{P_r^{(k-1/k)}}{P_r^{(k-1/k)} - 1}$$

and is a unique function of $P_r$. The Mach number distribution as a function of the radial coordinate is defined as

$$M(\bar{r}) = \left[\frac{\frac{2}{k-1}}{C\bar{r}^2(R_0/R_\infty)^2 - 1}\right]^{1/2} \tag{6}$$

The Mach number has the largest magnitude on the surface where the pressure is a minimum. The normalized velocity has a $(1/r)$ dependence expressed as

$$\bar{V}_\theta(\bar{r}) = \frac{V_\theta}{(kRT_0)^{1/2}} = \frac{\left(\frac{2}{k-1}\right)^{1/2}}{C^{1/2}(R_0/R_\infty)\bar{r}} \tag{7}$$

The integral continuity equation which provides a relation which defines $(R_\infty/R_0)$ for the fully expanded jet to atmospheric pressure is expressed as

$$R_0 \int_1^{(R_\infty/R_0)} \rho V_\theta \delta \bar{r} = \dot{m} \tag{8}$$

An analytical solution for $(R_\infty/R_0)$ which satisfies the continuity equation is expressed as

$$\frac{R_\infty}{R_0} = \left\{\frac{C\left[\left(C_{pt} + \frac{1}{P_r}\right)^{(1-k/k)} - 1\right]}{\left(C_{pt} + \frac{1}{P_r}\right)^{(1-k/k)}}\right\}^{1/2} \tag{9}$$

where

$$C_{pt} = \frac{P_{(R_0)} - P_\infty}{P_0}$$

is defined as the pressure coefficient, normalized on the total pressure. For $P_r$ less than critical, i.e., $P_r < (2/k+1)^{(-k/k-1)}$, then for uniform flow at the throat

$$C_{pt} = \frac{-A^*}{R_0}\left(\frac{2k}{k-1}\right)\left(\frac{1}{P_r}\right)^{(1/k)}\left[1 - \left(\frac{1}{P_r}\right)^{(k-1/k)}\right] \tag{10}$$

When the pressure ratio is greater than the critical, i.e., $P_r \geq (2/k+1)^{(-k/k-1)}$ when $M = 1$ at the throat, then the local normalized surface pressure to balance the centrifugal force is

$$C_{pt} = \frac{-A^*}{R_0} k\left[\left(\frac{2}{k-1}\right)\left(\frac{2}{k+1}\right)^{(k+1/k-1)}\right]^{1/2} \times \left[1 - \left(\frac{1}{P_r}\right)^{(k-1/k)}\right]^{1/2} \tag{11}$$

Figure 2 shows that $C_{pt}$ is linear with $A^*/R$, and a unique function of $P_r$. This analytical equation was derived from the momentum balance in the vertical direction, where the centrifugal force of the jet flow is balanced by the low pressure on the surface of the cylinder.

Figure 3 shows the analytical results of surface Mach number vs $P_r$ for six separate $A^*/R$ values. The curves reach an asymptotic limit dependent on $P_r$ at a fixed $A^*/R$. The physical

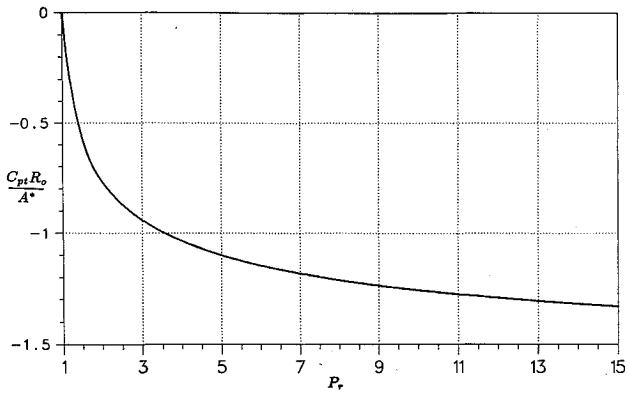


Fig. 2 Surface pressure coefficient to balance centrifugal force.

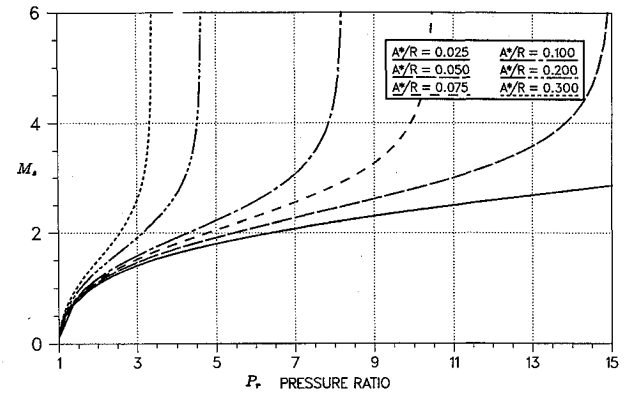


Fig. 3 Surface Mach number variation with $P_r$ for various $A^*/R_0$ values.

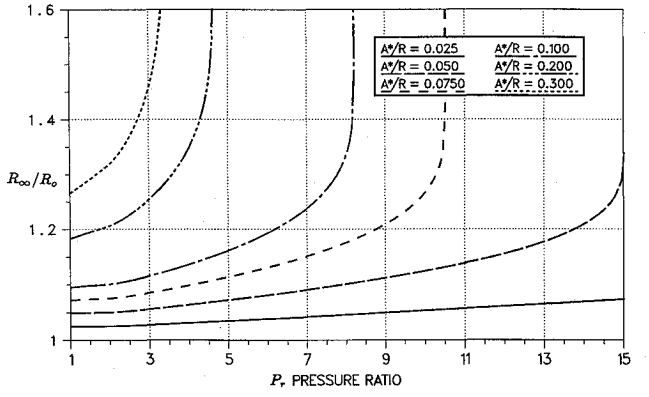


Fig. 4 Jet dimension increase for full expansion.

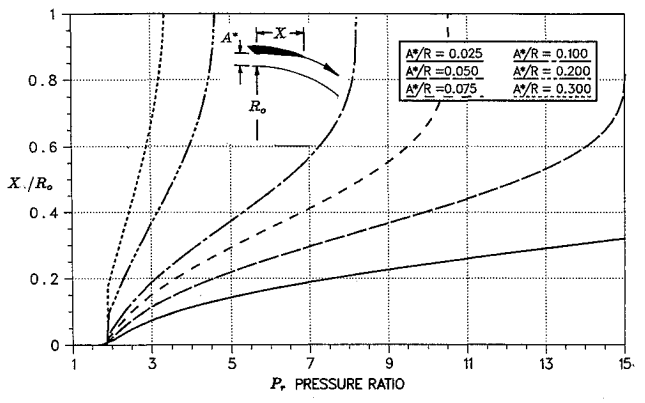


Fig. 5 Wall length extension for full expansion.

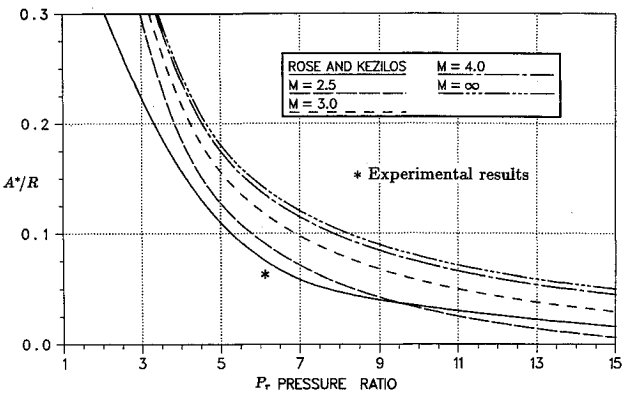


Fig. 6 Detachment criteria for underexpanded nozzle.

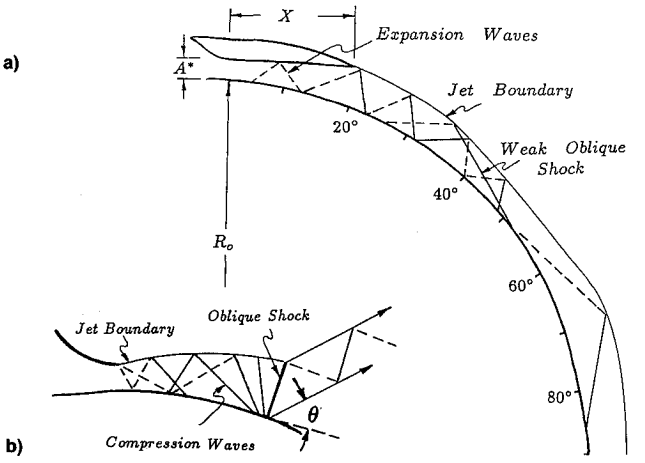


Fig. 7 Physics of supersonic Coanda flow: a) jet attached and b) jet detached at high $P_r$.

limit for a fixed $A^*/R$ occurs when $M = \infty$, when the surface pressure has reached the limit of absolute zero. Another experimental limit for air is the liquefaction of $O_2$ which occurs at $M = 3.6$ for a total temperature of 530°R. Since neither limit was approached for the experimental data, this was not considered to be a limiting factor. Figure 4 shows the analytical results for the fully expanded outer boundary of the jet $R_\infty/R$ vs $P_r$ for various $A^*/R$ values. The streamline which defines the fully expanded jet boundary increases to a large fraction of the initial radius for increasing $A^*/R$ values. Figure 5 shows the analytical results for the extended wall dimension necessary for the jet to become fully expanded for a radial distance between the surface cylinder and the outer wall. This wall extension provides for a converging-diverging nozzle geometry which was one of the parameters investigated in the experimental results section. Figure 6 shows the least squares curve fit for the experimental data[2] of $A^*/R$ vs $P_r$ for jet detachment. The experiment[2] was a compilation of Coanda jet detachment data for no external flow as a function of different diameter cylinders and jet heights at different $P_r$ values. The data correlated with the curve presented in Fig. 6, with a scatter of 25% in the experimental results. To demonstrate compressibility effects, the theoretical results for a constant surface Mach number were plotted on this graph. The jet detachment occurs when the surface Mach number from the analytical analysis is of the order of 2.5. The experimental data and the theory demonstrate the inverse relationship between $A^*/R$ and the $P_r$ to prevent jet detachment from the shock boundary-layer separation.

The above analytical results are strictly valid only for fully expanded $M \leq 1$. The results for $M \geq 1$ are considered to be qualitatively correct in describing the trends of surface Mach number with increasing $P_r$. For supersonic flow, the wave equation is the proper mathematical model for the Coanda

flow which produces an expansion and compression of the flow around the circumference of the cylinder. Figure 7b shows a sketch of the basic physics of the expansion and compressive waves in the supersonic region of an underexpanded nozzle flow around the cylinder. High-pressure air passes through the throat at a pressure of $P^*$ and $M = 1$, whereupon, the flow expands supersonically downstream between the area defined by the solid boundary and the outer shear layer. For an underexpanded nozzle, the pressure decreases downstream from $P^*$ at the throat from the supersonic expansion to the local atmospheric pressure. Due to the nature of the wave equation, the flow expands and then contracts as the expansion waves reflect off the shear layer as compressive waves. At the exit of the underexpanded nozzle, the flow streamline which defines the outer shear layer turns abruptly at the corner to the Prandtl Meyer expansion angle expressed as

$$\nu_{pe} = \sqrt{\frac{k+1}{k-1}} \tan^{-1} \sqrt{\frac{k-1}{k+1}(M^2-1)} - \tan^{-1}\sqrt{M^2-1} \tag{12}$$

Along this streamline the flow is supersonic and the flow is fully expanded to atmospheric pressure. As the $P_r$ increases, both the shear layer angle $\nu_{pe}$ and the corresponding Mach number increase. The Prandtl Meyer expansion around the upper corner produces a point source for the expansion waves which emanate from the singularity. Figure 7a shows the waves in the physical plane which demonstrate the expansion and compression process as waves from family *I* intersect and cross waves of family *II*. This problem is analogous to the classical underexpanded freejet physics.[14] The essential difference is the curvature of the surface streamline, which has the effect of producing an additional source for the expansion of the flow. The waves reflect from the solid surface as expansion waves which then impinge on the shear layer. The mechanics of the reflection of the waves from the shear layer result in the formation of compressive waves to satisfy the boundary condition of constant pressure along this streamline. Simultaneously, the outer shear layer turns toward the surface downstream, which reduces the shear layer angle to maintain a constant Mach number along the streamline.[14] At a sufficiently high $P_r$, the jet flow detaches from the surface as the flow transitions through an oblique shock. The shock position occurs within $x/A^* \sim 2.0$ along the solid cylindrical wall to satisfy the boundary conditions downstream from the shock. A schlieren photograph in Fig. 8 demonstrates that an oblique shock forms downstream at the $P_r = 7.6$, and the flow turns through an angle relative to the local surface curvature of the cylindrical surface. The physics of the flow expansion terminated by the oblique shock are shown in Fig. 7b. The mechanism which triggers the flow bifurcation is not well understood. Two states of the flow are possible near the critical $P_r$, the attached solution and the oblique shock mode which produces thrust vectoring of the jet downstream.

For the thrust vectored mode a simple explanation is proposed in terms of the integral momentum equation. The flow can be considered to be an isentropic expansion to the local static pressure before the shock position. The axial force $F_x$ remains constant for this problem. The side force $F_y$ is the net result of the pressure integration from the exit plane at the throat $P^*$ to the local atmospheric pressure $P_a$ along the length of the sidewall. The total force can be represented in terms of the vector contributions of axial and side force, where $F_t^2 = F_x^2 + F_y^2$. The vector diagram of the forces results in the following equation for the ratio of the side to axial force:

$$\frac{F_y}{F_x} = \left[\left(\frac{F_t}{F_x}\right)^2 - 1\right]^{1/2} \tag{13}$$

The maximum turning angle $\theta$ of the jet momentum is defined from the vector diagram of the force ratio, where the angle increases monotonically with $P_r$.

For CCW applications, the jet flow provides for boundary-layer control and super circulation for the airfoil geometry. The effective $P_{re}$ for the supersonic expansion of the jet flow is directly influenced by the $-C_p$ distribution downstream of the jet exit plane. This is demonstrated in Fig. 9 for the model surface pressure coefficient data[12] for a CCW of thickness-to-chord ratio of 0.156 for different blowing rates $C_\mu$. The blowing coefficient is independent of the local static pressure for choked flow and is defined as

$$C_\mu = \frac{\frac{4C_d}{k-1}[P_r^{(k-1/k)} - 1]\frac{A^*}{c}}{M_\infty^2} \tag{14}$$

The measured $-C_p$ on the cylinder surface downstream of the jet exit has a contribution from the centrifugal force of the jet, as well as the streamline curvature of the external flow above the jet. The pressure coefficient has two contributions which are defined as $C_p = C_{pj} + C_{pb}$. To segregate these effects, the contribution from the jet centrifugal force can be calculated from the graph in Fig. 2. The value of $C_{pb}$ represents the pressure coefficient for a streamline adjacent to the shear layer of the jet. The effective pressure ratio amplification which influences the jet expansion flowfield can be calculated from

$$(P_{re}/P_r) = \frac{1}{[C_{pb}(kM_\infty^2/2) + 1]} \tag{15}$$

The results of the amplification are plotted in Fig. 10 for various values of $C_{pb}$ vs the freestream Mach number, where

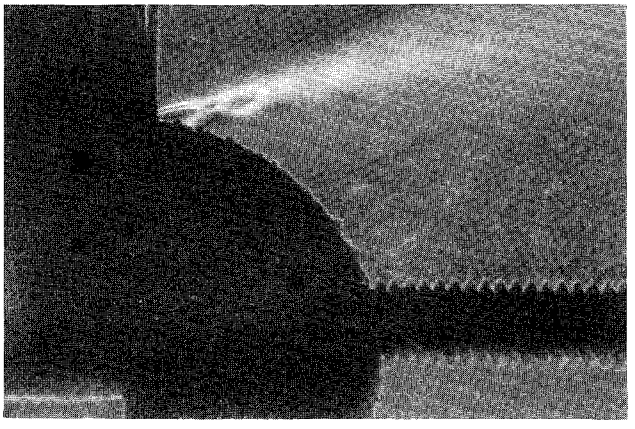

Fig. 8 Schlieren photograph at $P_r = 7.8$ terminated by oblique shock.

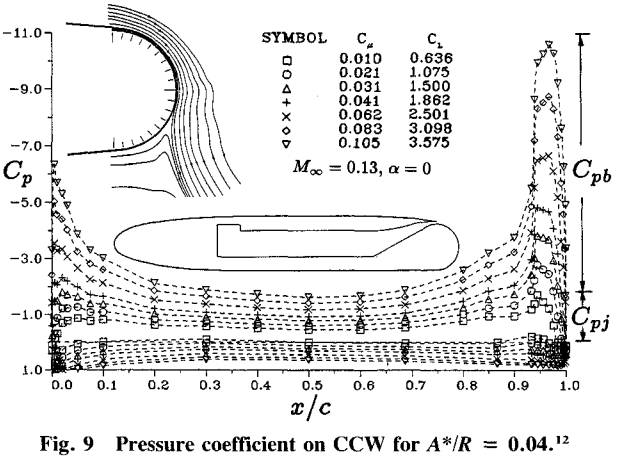


Fig. 9 Pressure coefficient on CCW for $A^*/R = 0.04$.[12]

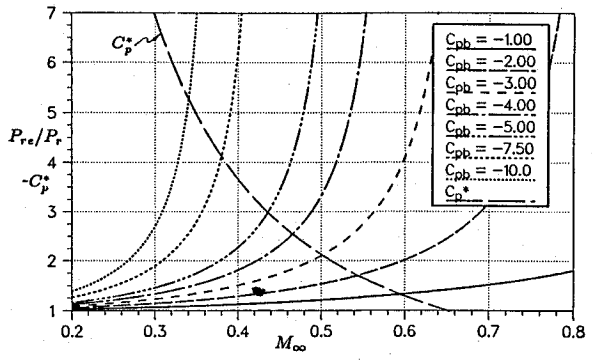


**Fig. 10 Pressure ratio amplification from local exterior static pressure.**

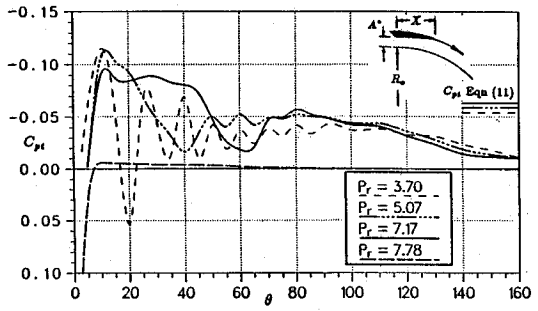


**Fig. 11 Experimental surface pressure coefficient for $A^*/R$ = 0.04, $X/A^*$ = 0.0.**

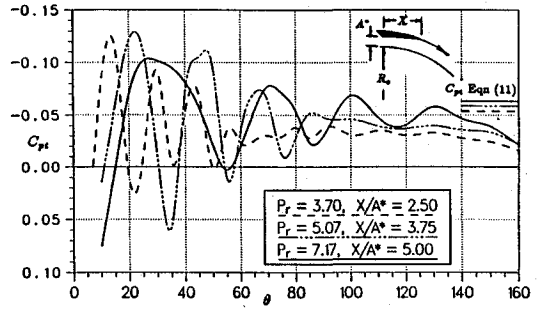


**Fig. 12 Experimental surface pressure coefficient for extended wall, $A^*/R$ = 0.04.**

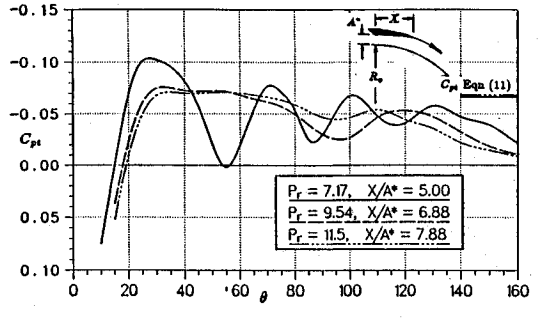


**Fig. 13 Experimental surface pressure coefficient with wall extension, $A^*/R$ = 0.04.**

the parameter $P_r$ was calculated from the tunnel static pressure. For a Mach number of 0.3 and $C_{pb}$ = −9.2, an amplification of magnitude 2.3 was calculated for the effective $P_{re}$. The critical pressure coefficient is also plotted in Fig. 10, demonstrating the maximum allowable $C_{pb}$ for a streamline which reaches sonic velocity above the jet. If there is a sonic region of flow above the jet boundary, the physics of the jet turning are altered, producing stall[5] of the flow on the airfoil with increased $C_\mu$. For the supersonic freejet to remain attached around the cylinder, the expansion waves must reflect from the density gradient at the interface of the shear layer.

## Experimental Results

### Underexpanded Freejet

The data of normalized surface pressure that is presented in Fig. 11 confirm large fluctuations between positive and negative pressure coefficients for underexpanded jets. The oscillating pattern is evident from the data which demonstrate that $C_{pt}$ approaches a minimum below zero and then oscillates downstream from the physical interaction of the expansion waves and the focusing of the compression waves. The growth in magnitude of the oscillations commences at a $P_r \sim 3.0$. When the $P_r$ reaches a value of 7.6, the oblique shock mode dominates above this $P_r$ threshold and the jet is vectored from the surface. The schlieren photograph in Fig. 8 demonstrates that an oblique shock forms within 2.0-slot heights downstream at the $P_r$ = 7.8.

The distance from the minimum pressure to the maximum represents the half-wavelength of the supersonic expansion before the wave pattern repeats as the compressive waves converge downstream. This length is a function of the surface Mach number as the flow expands downstream until the wave mechanics at the shear layer interface are satisfied. The experimental results for higher $P_r$ values show an increase in the first peak-to-peak wavelength with increasing $P_r$. At a fixed $P_r$, the wavelength decreases downstream, reflecting the dissipation of energy with the local Mach number decreasing. The entropy increase is attributed to the reflections of the waves from the time varying shear layer, which translate to fluctuations of both velocity and density. A time-averaged turbulence production would be generated throughout the entire jet domain. Most of the entropy effects occur downstream as the compressive waves are reflected from the shear layer. This feature of the underexpanded jet accelerates the transition to the strong oblique shock and the departure of the jet from the surface. Eventually, at a higher $P_r$, the inviscid wave equation does not support an attached flow solution and the flow transitions through an oblique shock to satisfy the boundary conditions. It is hypothesized that this characteristic of the flow expansion undoubtedly limits the slot blowing effectiveness at higher $P_r$ values.

### Extension of Upper Wall

By traversing the upper wall over the cylinder, the supersonic expansion is contained between the solid boundaries. Figures 12 and 13 show the surface pressure coefficient data for various extensions of the upper wall at different $P_r$ values. The upper wall extensions $X/A^*$ were selected from Fig. 5 which exhibited the largest turning angle of the Coanda jet. At a $P_r$ = 11.5, the wall jet boundary-layer separates at $\theta \sim$ 150 deg around the circumference of the cylinder. Figure 14 shows the schlieren photograph demonstrating that the jet remains attached to the surface at $P_r$ = 11.5. This was the highest $P_r$ that could be obtained in the laboratory. One of the advantages of the upper wall extension is that it prevents the flow from expanding to the Prandtl Meyer expansion angle. The solid wall also prevents the waves from reflecting from the time varying shear layer during the supersonic expansion process through the throat. The pressure oscillation magnitude when normalized on the total pressure is less for the higher $P_r$ values, demonstrating a smaller magnitude in the adverse pressure gradient which should have less impact on the surface boundary layer growth. Figures 15 and 16 show the experimental data for a fixed $x/A^*$ = 5.0 at different $P_r$ values which demonstrate the off design performance at lower $P_r$ with the design $P_r$ = 7.1. Fortunately, with the wall extension designed for higher $P_r$, there is no significant degradation of the ability of the supersonic jet flow to remain attached around the cylinder at the lower $P_r$ values. The boundary layer fortuitously separates from the upper straight wall rather than the cylindrical surface for $P_r$ below the design condition, i.e., above a $P_r$ = 2.0 at the $A^*/R$ = 0.04 for the

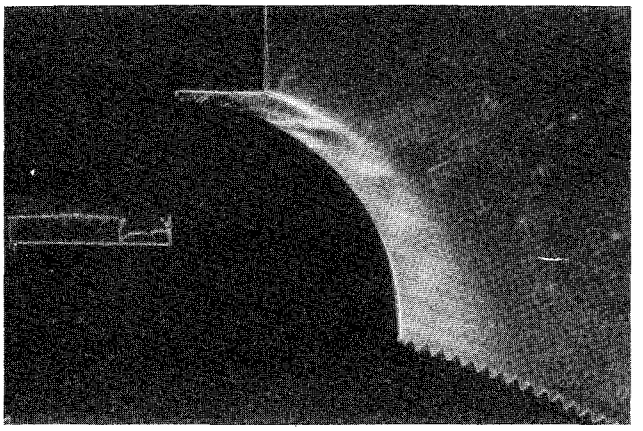

**Fig. 14 Schlieren photograph of supersonic Coanda flow, $P_r$ = 11.5, $A^*/R$ = 0.04, $X/A^*$ = 7.0.**

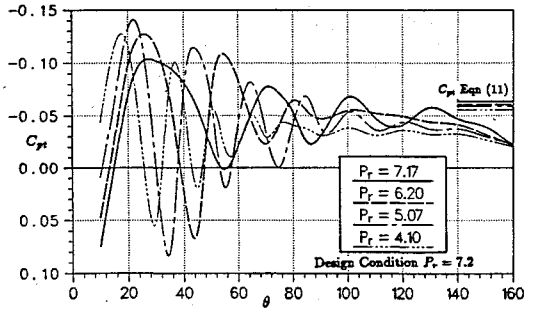


**Fig. 15 Off-design performance for $x/A^*$ = 5.**

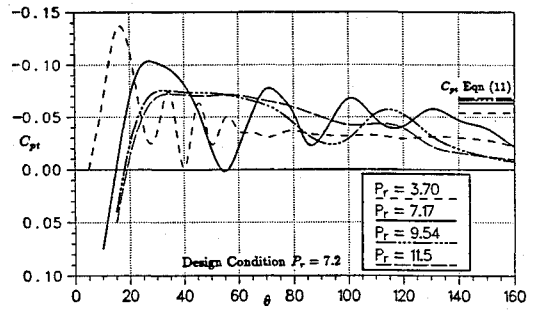


**Fig. 16 Off-design performance for $x/A^*$ = 5.**

experimental data for the static blowing conditions investigated in this research.

## Concluding Remarks

An experiment was undertaken to measure the wall static pressure variation from an underexpanded nozzle flow around a cylindrical surface to quantify the jet detachment physics. The theory predicts a physical upper limit of $A^*/R$ for a finite $P_r$ which occurs when the surface Mach number approaches infinity. Before this limit is reached at a sufficiently high $P_r$, the wave equation cannot support an attached solution, and the jet flow transitions through an oblique shock which vectors the jet momentum at an angle relative to the surface curvature. The experimental data for the two-dimensional jet detachment criteria show that an oblique shock forms which vectors the jet from the surface. A correlation with the approximate inviscid compressible flow theory demonstrates that this phenomena occurs when the surface Mach number approaches a value $M_s$ = 2.5. The experimental curve and the theory demonstrate the inverse relationship between the physical parameter $A^*/R$, and the $P_r$ to prevent shock boundary-layer separation.

The simple geometry of an underexpanded jet with a wall extension above the cylindrical surface shows that a higher $P_r$ can be attained before jet detachment. When the optimum extension of the wall for the higher $P_r$ was maintained at a fixed value, the data at lower $P_r$ were not degraded, and the jet turning was not effected. The data demonstrate that for the two-dimensional converging-diverging nozzle, a large magnitude in the turning angle can be obtained, which shows the efficient turning for this configuration. For the two-dimensional converging-diverging nozzle, the optimum length of the upper wall which dictates the area expansion ratio to the exit plane increases monotonically with $P_r$. For practical applications there is an advantage to keeping the jet attached at higher $P_r$. A large range of $P_r$ allows flexibility in the variation of the $C_\mu$ for scaling to higher subsonic Mach numbers for both CCW and pneumatic forebody blowing applications. When the jet has expanded to the maximum dimension, the radius of curvature for a streamline outside the jet boundary will increase, thus delaying sonic conditions along this streamline at a higher freestream Mach number. Higher $P_r$ also translates to a reduction in size of the pneumatic lines which would be routed from the compressor stage of the gas turbine.

## Acknowledgments

This research was partially funded under Contract F33601-89-D0045 from the Flight Dynamics Laboratory, Wright Patterson Air Force Base, Dayton, Ohio, with additional support through the Wright State University research incentive funds. The authors would like to acknowledge the helpful discussions with Russ Osborne from the Aeromechanics Division.

## References

[1]Kizilos, A. P., Kizilos, B. M., and Smith, G. A., "Study of Blowing Transverse Jets from Airfoils for Flight Control Applications in the Mach Number Range 0.2 to 3.0," Honeywell Inc. Doc. 12146-FR, prepared under Contract N00019-69-C-0286 for Naval Air Systems Command, Dept. of the Navy, Nov. 1970.

[2]Kizilos, A. P., and Rose, R. E., "Experimental Investigations of Flight Control Surfaces Using Modified Air Jets," Honeywell Inc. Doc. 12055-FR1, prepared under Contract N00019-69-C-0286 for Naval Air Systems Command, Dept. of the Navy, Oct. 1968.

[3]Seed, A. R., "Detachment of Wall Jets from Curved Surfaces," National Gas Turbine Establishment, Pyestock, Hants, England, UK, April 1969.

[4]Kind, R. J., "A Proposed Method of Circulation Control," Ph.D. Dissertation, Clare College, Cambridge Univ., 1967.

[5]Rogers, E. O., "Development of Compressible Flow Similarity Concepts for Circulation Control Airfoils," AIAA Paper 87-0153, Jan. 1987.

[6]Wood, N. J., and Conlon, J. A., "The Performance of a Circulation Control Airfoil at Transonic Speeds," AIAA Paper 83-0083, Jan. 1983.

[7]Wood, N. J., and Nielsen, J. N., "Circulation Control Airfoils Past, Present, Future," AIAA Paper 85-0204, Jan. 1985.

[8]Abramson, J., and Rogers, E. O., "High-Speed Characteristics of Circulation Control Airfoils," AIAA Paper 83-0265, Jan. 1983.

[9]Englar, R. J., "Two-Dimensional Transonic Wind Tunnel Tests of Three 15-Percent Thick Circulation Control Airfoils," Naval Ship Research and Development Center TN AL-182; AD 882-075, Dec. 1970.

[10]Lowry, J. G., Riebe, J. M., and Campbell, J. P., "The Jet-Augmented Flap," 25th Annual Meeting of the Inst. of the Aeronautical Sciences, Paper 715, New York, Jan. 1957.

[11]Englar, R. J., and Williams, R. M., "Test Techniques for High Lift Two-Dimensional Airfoils with Boundary Layer and Circulation Control for Application to Rotary Wing Aircraft," *Canadian Aeronautics and Space Journal*, Vol. 19, No. 3, 1973, pp. 93–108.

[12]Novak, C. J., and Cornelius, K. C., "An LDV Investigation of a Circulation Controlled Airfoil Flowfield," AIAA Paper 86-503, Jan. 1986.

[13]LeMay, S. P., Sewall, W. G., and Henderson, J. F., "Forebody Vortex Flow Control on the F-16C Using Tangential Slot and Jet Nozzle Blowing," AIAA Paper 92-0019, Jan. 1992.

[14]Shapiro, A. H., *The Dynamics and Thermodynamics of Compressible Fluid Flow*, Vol. 1, Wiley, 1953, pp. 450–490.